Available online at www.sciencedirect.com
ScienceDirect
Journal of Power Sources 163 (2007) 960–965
JOURNAL OF POWER SOURCES
www.elsevier.com/locate/jpowsour

Short communication

Short-period segmented-in-series solid oxide fuel cells on flattened tube supports

Manoj R. Pillai [a], Dan Gostovic [a,1], Ilwon Kim [a], Scott A. Barnett [a,b,*]

[a] *Functional Coating Technology LLC, 1801 Maple Avenue, Evanston, IL 60201, United States*
[b] *Materials Science and Engineering, Northwestern University, Evanston, IL 60208, United States*

Received 13 July 2006; received in revised form 28 September 2006; accepted 29 September 2006
Available online 15 November 2006

Abstract

Segmented-in-series solid oxide fuel cells (SIS-SOFCs) were prepared on flattened-tube partially stabilized zirconia supports. The distinguishing characteristic of these cells was the short repeat period, 2.4 mm, and small active cell length, 1.3 mm, compared to ≈10 mm in previous SIS-SOFCs. The support tubes, formed by gelcasting, were bisque fired and then screen printing was used to sequentially deposit Ni-YSZ anodes, YSZ electrolytes, and Pt-YSZ composite interconnects. After high-temperature co-firing, LSM–YSZ and LSM cathode layers were screen printed and fired. Each flattened tube side had 12–16 individual cells. For testing, the open tube ends were sealed and humidified hydrogen flowed inside of the tubes; air was flowed over the outside of the tubes. Maximum total power at 800 °C was ≈8 W and maximum power density was ≈0.7 W cm^{-2}, calculated using cell active area. Good stability was observed during a ≈650 h steady-state test. Excellent stability was also observed over ≈20 redox cycles.

Keywords: Solid oxide fuel cells; Gelcasting; Screen printing; Segmented-in-series; Redox cycling; Multi-cell stack

1. Introduction

Recent calculations for segmented-in-series solid oxide fuel cells (SIS-SOFCs) have indicated that power densities approaching 1 W cm^{-2}, comparable to planar SOFCs, can be achieved by using cell lengths of ≈1–2 mm [1]. These small lengths are needed to provide low lateral electrode resistances when using relatively thin (20–50 μm) electrodes that are readily prepared by screen printing. For more traditional SIS-SOFCs where cell widths are typically ≥10 mm [2–4], such high power densities are typically not achieved, and indeed would only be feasible with very thick (≈1 mm) perovskite (e.g. LSM) cathodes, or alternatively by using highly conductive precious-metal-containing cathodes [5].

While good performance is possible, fabricating SIS-SOFCs with 1–2 mm cell lengths is challenging. It requires feature resolution and alignment accuracy of ≈0.1 mm, near the limit of what can be achieved by patterned deposition techniques such as screen printing. Recent demonstrations of short-length SIS-SOFCs are promising but have been limited to four-cell arrays on planar supports with <1 cm^2 active cell area [6,7]; an important next step is to demonstrate fabrication and good performance for larger areas with larger numbers of cells. It is also necessary to demonstrate this concept in a more useful geometry, e.g. flattened tubes with cell arrays on both sides.

In this paper, we report results from SIS-SOFC modules with segmented-in-series arrays screen printed on both sides of flattened partially stabilized zirconia (PSZ) tubes. A conventional SOFC materials set – Ni-YSZ anodes, YSZ electrolyte, and LSM–YSZ cathode – was employed along with a Pt-YSZ composite interconnect. The processing included high-temperature co-firing of the support, anode, electrolyte, and interconnect, followed by application and firing of the cathode. The arrays covered a total print area of ≈12–16 cm^2 (depending on the length of the tube) on each tube side, had ≈12–16 cells on each side with an active cell length of 1.2–1.3 mm, and an interconnect length of 0.2 mm. A maximum power density (calculated using active cell area) of ∼700 mW cm^{-2} was measured at 800 °C. Stable operation over ≈650 h was demonstrated. Moreover, excellent array

* Corresponding author. Tel.: +1 847 491 2447; fax: +1 847 491 7820.
E-mail address: sbarnett@fctnet.com (S.A. Barnett).
[1] Present address: Department of Materials Science and Engineering, University of Florida, Gainesville, FL 32611, United States.

0378-7753/$ – see front matter © 2006 Elsevier B.V. All rights reserved.
doi:10.1016/j.jpowsour.2006.09.079

performance stability was measured over ≈20 redox cycles, presumably due to the small thickness of the Ni-YSZ anodes.

2. Tube fabrication and experimental methods

2.1. Gelcasting of PSZ support tubes

A gelcasting slurry was prepared by ball milling PSZ powder (TOSOH) and starch (pore former) along with a monomer (hydroxy ethyl methacrylate), dispersant, and water as the solvent. An initiator along with a catalyst was then added to the slurry to start the gelling process [8]. The catalyst, along with a slightly elevated temperature (∼70 °C), helped to reduce the gelling time. The slurry was then poured into a mold. After gelation, the mold internal parts were removed and the support tubes dried slowly. Finally, the green tubes were pre-fired, typically at 1150 °C, in order to burn off the organics and provide sufficient strength for handling and screen printing.

2.2. Screen printing and firing

Screen printing was employed to deposit the electrodes, electrolyte, and the interconnect layers. The screen printing inks were prepared by first ball milling the relevant powders, and then combining with vehicle (Electro-Science Laboratories 450 and/or V 737, Heraeus Inc.) in a three-roll mill. Prints with excellent uniformity and well-defined patterns with resolution <100 μm were reproducibly obtained. Details of the screen printing – e.g. ink solids loading and rheology, adjustment of the printer parameters, and surface flatness requirements – have been described previously [9]. Layer thicknesses were varied via parameters including ink viscosity, solids loading, screen mesh size, and number of prints.

The anode material was Ni-YSZ cermet. NiO (J.T. Baker) and YSZ (TOSOH) were mixed in the weight ratio 70:30, before ink fabrication with solids loading of ∼20–25% by volume. Final anode thickness was ≈20 μm. The electrolyte was YSZ with 8% Y_2O_3 obtained from TOSOH. A solids loading of ∼25% was used, yielding a thickness of ≈20 μm. The interconnect was made from a mixture of Pt (Technic Inc.) and YSZ in the volume ratio of 45:55. The ink solids loading was ≈20% by volume, yielding a thickness of ≈30 μm. The above three layers were all printed in sequence with drying between the print steps. This procedure was then repeated on the other side of the flattened tube. High-temperature firing was done at 1400 °C. After firing, the support porosity measured by the Archimedes' method was ≈43%, The interconnect resistivity, measured separately using un-patterned layers at room temperature using a van der Pauw geometry, was $\approx 10^{-4}\ \Omega$ cm.

Matching of the cathode screen to the pre-existing anode/electrolyte/interconnect patterns was a key issue because of the shrinkage that occurred during the high-temperature firing step. The support shrinkage was typically ≈19–20%. The shrinkage variation between different supports fired using the same procedure was consistently less than 0.5%. This relatively small variation made it possible to match the cathode screen print to the as-fired patterns. The cathode was a mixture of LSM (Praxair) and YSZ in the ratio 50:50 by weight. The solids loadings of both the LSM–YSZ and the LSM inks were about 28%. After printing and drying the LSM–YSZ cathode layer, it was fired at 1175 °C for 1 h. Two consecutive LSM current collector prints were then done and fired at 1125 °C for 1 h in order to produce an 80–100 μm thick layer; the thick current collector helped minimize cathode resistance losses as described elsewhere [1].

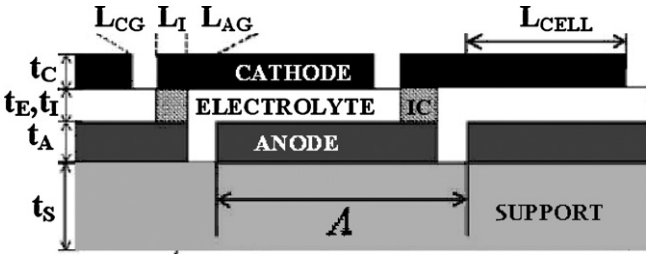

Fig. 1. Schematic drawing showing the geometry of the segmented-in-series SOFC array (adapted from Ref. [1]). Dimensions shown are the cell period Λ, active cell length L_{cell}, cathode gap L_{CG}, anode gap L_{AG}, interconnect length L_I and thickness t_I, electrolyte thickness t_E, anode thickness t_A, cathode thickness t_C, and support thickness t_S.

Fig. 1 shows schematically the lateral dimensions and alignment of the printed layers after completed fabrication. Note that Fig. 1 is somewhat idealized: the interconnect was actually wider than the gap in the YSZ electrolyte, extending 150–200 μm beyond either side of the gap to ensure that the electrolyte/interconnect combination provided a continuous dense layer. The cells were 4 cm wide, yielding an active area per cell of ≈0.5 cm^2. The percentage of the print area that was active fuel cell (defined by the anode–cathode overlap as shown in Fig. 1) was ≈52–55%.

Fig. 2 shows an image of a finished module, illustrating the flattened tube geometry with cross-members and a 15-cell array

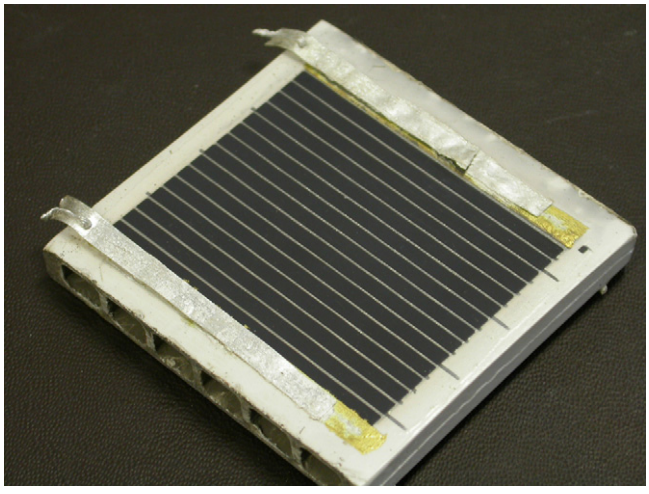

Fig. 2. Optical image of a typical screen printed segmented-in-series SOFC module after electrical testing. The black strips visible on the flattened PSZ tube are the cathodes of individual cells. The PSZ tube interior has cross ribs both for strength and to provide channels for fuel flow. The silver strips visible on both ends were used for electrical connections to the end electrodes of the array.

on each side. After firing, the modules were ≈5 cm × 5 cm, and the printed area was ≈3.6 cm × 4 cm.

2.3. Module testing setup

The completed module was held between two stainless steel manifolds that were sealed to each of the module open ends. A combination of mica and Ag ink was used for sealing between the manifolds and the module ends. Pressure was applied for sealing using the threaded rods and wingnuts via springs. One manifold was used as the fuel inlet and the other used for the exhaust gas. Evenly spaced holes in the manifolds were used to supply fuel to the SIS-SOFC module gas channels. Electrical connections were made along the full length of the first and last electrodes of the arrays using silver ink, strips (Fig. 2), and wires. Two wires were connected to each end electrode: one for current and the other for voltage measurement.

The modules were tested in a split tube furnace. During testing, humidified hydrogen was supplied at a flow rate of 500 sccm with 600 sccm of air at the cathode surface. Initially, the Ni-based anodes were reduced in hydrogen at 800 °C for ≈2 h. Current and voltage were measured using a Keithley-2440 5 A power supply that was interfaced to a computer using a GPIB card. The electrochemical impedance spectra were obtained using an IM6 Electrochemical workstation (Zahner, Germany). The frequency range studied was from 100 kHz to 100 mHz. The IM6 supplied a current through the two current wires and the voltage was measured by two separate voltage wires.

3. Results and discussion

3.1. Microstructure and permeability measurements

Fig. 3a shows a representative fracture cross-sectional SEM image of the electrolyte portion of a completed SIS-SOFC. Fig. 3b shows a similar image of the interconnector region. In both images, the layers are reasonably flat and uniform, with intimate contact at the interfaces. Fig. 3c shows a lower magnification image of the transition region between the electrolyte and interconnect. Note that there was a ≈200 μm-wide region where the interconnect overlapped the electrolyte. The support shows large pores due to the pore former. The electrode layers show the expected porosity while the electrolyte appears to be reasonably dense. The interconnect layer showed considerable structure since it consisted of Pt and YSZ phases, so it was difficult to ascertain whether it was dense from these images. These images and other low magnification plan-view SEM images showed that the layers were free of large holes or defects. On the other hand, plan-view SEM images of the Pt-YSZ interconnect surface (Fig. 3d) showed small open pores that may be a source of gas leakage. For comparison, the screen printed YSZ surfaces showed no such pores.

Leak tests across these layers were carried out by doing unpatterned large-area screen prints on PSZ surfaces and firing under conditions identical to those used for printing the modules. The measurement provided a qualitative measure of leak rate by pumping on one side of the layer with a mechanical vac-

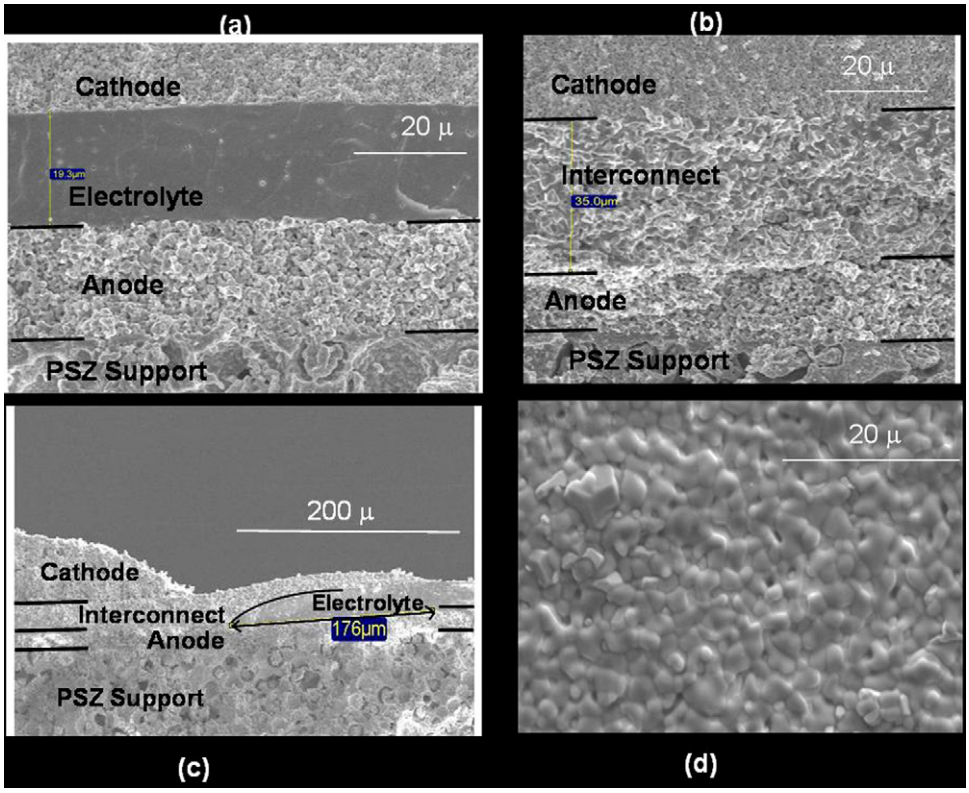

Fig. 3. Representative SEM images of the SOFCs. (a) Cross-sectional image of a region showing the support, anode, electrolyte, and cathode. (b) Cross-sectional image of a region showing the support, anode, interconnect, and cathode. (c) Lower magnification cross-sectional image showing the region between cells where the interconnect and electrolyte overlap. (d) A plan-view image of the interconnect surface showing small open pores.

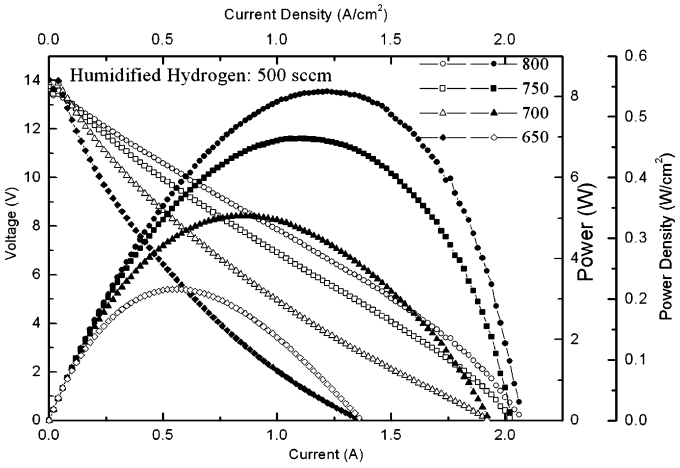

Fig. 4. Voltage and power vs. current from a segmented-in-series module with 15 cells on each side. Also shown are the current density and power density calculated based on active cell area. The module was tested at different temperatures with air at the cathodes and humidified hydrogen at the anodes.

uum pump, and using a vacuum gauge to measure the pressure achieved. The vacuum chamber yielded an ultimate pressure of 0.2 Torr when the sample was fully dense. Good quality screen printed YSZ layers typically yielded pressures from 0.2 to 0.3 Torr. Permeability measurements [9] on a Pt-YSZ surface screen printed on a gelcast PSZ piece and fired at 1400 °C gave ultimate pressures of 0.9 Torr. Prior measurements on planar SOFC button cells with a similar leak tester showed that this pressure level was sufficient to deleteriously impact open-circuit potential [9]. Thus, the Pt-YSZ layers appeared to be a source of leakage in these SOFC modules.

3.2. Electrical performance

Fig. 4 shows electrical test results from one of the modules tested (module A), with 15 cells on each side and the two sides electrically connected in parallel. Results are shown at various temperatures with humidified hydrogen supplied to the anodes at a flow rate of 500 sccm, and air flowed outside the module. The maximum module power output was 8 W (535 mW cm^{-2} calculated using active cell area) at 800 °C and 7 W (465 mW cm^{-2}) at 750 °C. The current–voltage curves were fairly typical of thin-electrolyte SOFCs with these materials operated in this temperature range [10]. At lower temperature, the voltage versus current was concave up, indicating that activation polarization dominated the cell performance. At higher temperature, the voltage versus current became more linear – probably indicating that ohmic resistance was becoming more important – and there were indications of concave-down curvature, perhaps indicating concentration polarization at a current density of ≈2 A cm^{-2}. The average cell area-specific resistance, obtained from the *I–V* curves (open-circuit voltage divided by short circuit current density) varied from ≈0.4 Ω cm^2 at 800 °C to ≈0.7 Ω cm^2 at 650 °C.

These values were typical of the segmented-in-series modules tested with the two sides electrically connected in parallel. When the sides were measured separately, higher power (usually a 5–10% difference) was observed from the SOFC array on one side. One of the best modules (module B) tested so far gave maximum power densities of ≈700 mW cm^{-2} on one side and 650 mW cm^{-2} on the other at 800 °C, corresponding to area-specific resistances of 0.26 and 0.29 Ω cm^2, respectively. This was probably due to slight variations in the processing steps involved in fabricating the two sides, including the fact that the second side printed had a thinner cathode due to one fewer LSM print. There may also have been some variations in the quality of the end contacts on each SOFC array.

The open-circuit voltage, ≈14 V across 15 cells in Fig. 4, corresponded to 0.93 V per cell, substantially lower than the theoretical value of ≈1.1 V per cell in humidified hydrogen and air. This was fairly typical of OCV values measured for the segmented-in-series modules, which ranged from 0.91 to 0.96 V per cell at 800 °C. We attribute the low OCV to gas leakage, probably through both the module end-seals and the Pt-YSZ interconnects. Leakage at the end-seals was verified in tests with dense "dummy" modules, by observing that the gas out-flow rate was ≈15% less than the inlet flow rate. The interconnects were suspect because the out-flow rate was further reduced by ≈25% when actual modules were tested. This is consistent with the vacuum leak-rate measurements described above. The OCV may also be reduced slightly (<10 mV) due to residual ionic conductivity in the PSZ supports that allows a small parasitic support current [1].

The fuel utilization in most of the modules tested was ≈20–25% at maximum power at 800 °C. Attempts to improve the utilization by decreasing the fuel flow rate had limited success. For example, a decrease from 500 to 200 sccm in module B increased the utilization only to 30%, because the maximum power density decreased from 650 to 460 mW cm^{-2}. This was due more to a change in module current – the short circuit current decreased by ∼50% when the flow rate was reduced to 200 sccm – than to a decrease in OCV—which decreased by only ∼5%. This probably indicates increased concentration polarization at the down-stream cells as H_2 was depleted by oxidation and leakage. Based on these results, an increase in the density of the interconnect is a key need for these modules; improved leak tightness would not only allow higher fuel utilization but increase OCV values, which would in turn increase power density.

Fig. 5 shows the AC impedance spectrum at various temperatures from one side of a module (module C) that had eight cells on both sides. Humidified hydrogen at flow rate of 200 sccm was used as the fuel. The measured resistances were divided by the number of cells (8) and multiplied by the active area per cell (0.5 cm^2) to yield the area-specific resistances plotted. At each temperature, the electrode arc was substantially larger than the high-frequency horizontal-axis intercept, indicating that electrode polarization was the main component of the cell losses. There were three apparent electrode arcs: a very small arc at the highest frequencies, a large arc at moderate frequencies, and a smaller arc at the lowest frequencies. The general frequency ranges and sizes of these arcs are similar (except for the highest-frequency arc) to those reported for planar thin-electrolyte SOFCs with the same materials set as in the present experiments [11]. The decrease in the high-frequency

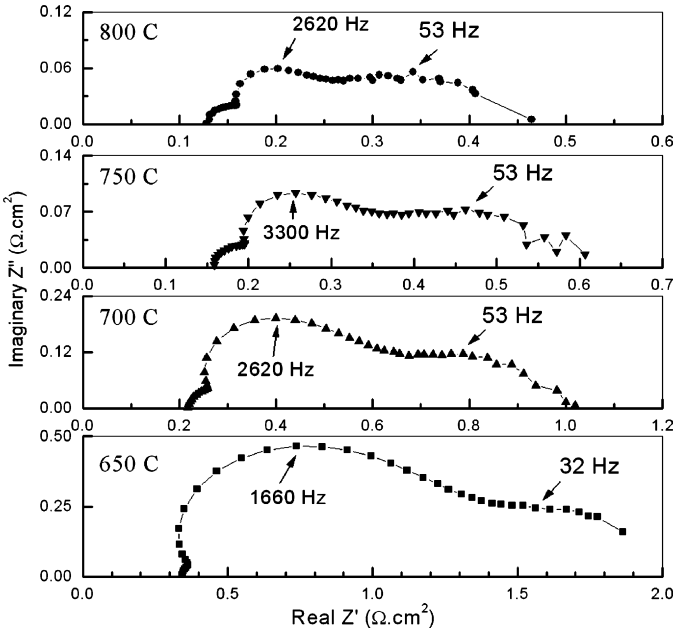

Fig. 5. Electrochemical impedance spectra measured at different temperatures across eight series-connected cells on a segmented-in-series module. Measurements were done at open circuit with air at the cathodes and humidified hydrogen at the anodes. Frequencies at the tops of the arcs are labeled.

intercept with increasing temperature, e.g. from 0.34 Ω cm^2 at 650 °C to 0.15 Ω cm^2 at 750 °C, was consistent with the area-specific resistance expected for a 20 μm-thick YSZ electrolyte at these temperatures [12], 0.47 Ω cm^2 at 650 °C to 0.13 Ω cm^2 at 750 °C. The change from 750 to 800 °C was less, however, and the predicted value of 0.08 Ω cm^2 at 800 °C [12] was considerably lower than the measured value of 0.12 Ω cm^2. This indicates another component of ohmic loss that may be related to the interconnects, lateral resistance losses across the electrodes, and contact/wire measurement losses. We suspect that the interconnect losses were unimportant here, because of the high conductivity of the Pt-YSZ. A substantial portion may be the contact/wire losses, as good NiO–YSZ anode-supported cells tested in our lab, with no interconnect or lateral electrode losses, typically show a similar ohmic resistance of ≈0.1 Ω cm^2 at 800 °C [9,13]. Overall, these results suggest that the present segmented-in-series design succeeded in achieving relatively low electrical resistance losses. Electrode polarization resistances were the primary losses, so attempts to improve module performance should focus primarily on this area.

3.3. Stability testing

The SOFC modules generally showed stable performance. Fig. 6 shows the voltage versus time from one side of a module that was operated at 460 mA at 750 °C. The break in the data at ≈320 h was due to a computer malfunction. The slight increase in performance observed after the break was due to resumption of air flow that had stopped at some point during the first 300 h. Despite these flaws in the life test, the overall stability was good, with ≈3.5% reduction in voltage over ≈700 h. Note that some of this degradation was likely due to the test apparatus; especially

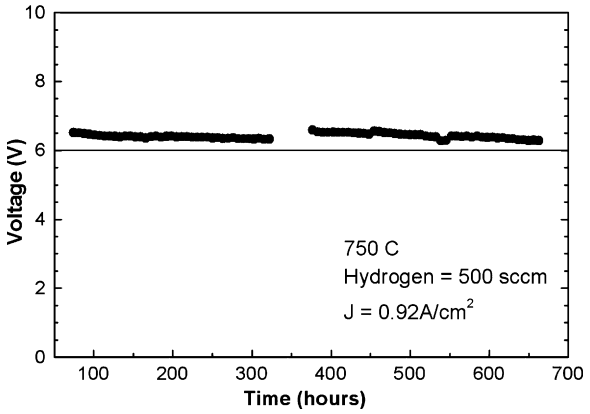

Fig. 6. Voltage vs. time for a segmented-in-series module maintained at a constant current density of 0.92 A cm^{-2}. The measurement was made from 12 cells on one side of the module. The break in the data around the 350 h point was caused by a failure in the testing electronics. Some of the voltage decrease in the first 350 h was due to a loss of air flow to the cathode; when testing was resumed after the break, the air flow was re-started and the voltage was increased. The line at 6 V was added to guide the eye.

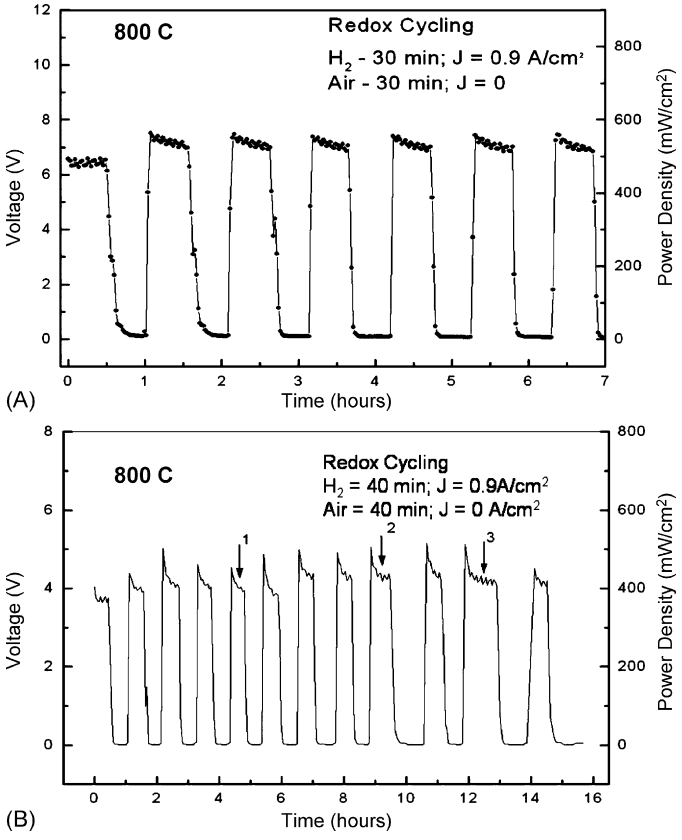

Fig. 7. Cell voltage vs. time at constant current (while hydrogen was flowing) during redox cycling at 800 °C. In the first part of the test shown in (A), 12 cells on one side of the module were tested during 7 cycles. The module was cycled to room temperature and then back to 800 °C before the second part of the test (B), where 9 cells on the other side of the module were tested during 12 cycles. Arrows 1 and 2 indicate when the module was left overnight at 800 °C in hydrogen without cycling. Arrow 3 indicates a longer-than-usual (1 h) fuel cycle.

because the Ag ink and wires tend to degrade over the time scales of this test.

Fig. 7 shows the effect of redox cycling on SIS-SOFC performance. In the initial test shown in Fig. 7A, module B was operated under typical conditions, 500 mW cm^2 at 800 °C, for 30 min before the fuel flow was stopped and air flowed through the module for 30–40 min. The fuel flow was then re-started and the cycle repeated seven times. The voltage spiked immediately after re-starting the fuel flow in each cycle, but then approached to a saturation value near the initial power level. Overall, however, there was no apparent cycle-to-cycle degradation. The module was then cooled to room temperature and then re-heated back to 800 °C for a second set of redox cycles. Fig. 7B shows the second set of 12 redox cycles (with two breaks of ∼15 h each), in this case measuring the other side of the same module. The test conditions were the same as in the previous test, as were the results, although the power output was lower from this side of the module. Note that cycle 11 was run longer in the fuel cell mode, 60 min, showing more clearly that the voltage reached a steady-state value. These results show excellent redox cycling tolerance over a total of 19 cycles, much better than observed for Ni-YSZ anode-supported SOFCs [14]. This is presumably due to the small amount of Ni in the thin SIS-SOFC anodes compared to anode-supported SOFCs. Thus, there appears to be little structural degradation to the anode caused by the expansion and reduction as the anode Ni was oxidized to NiO and then back to metallic Ni [15].

4. Summary and conclusions

The above results demonstrate the fabrication of short-period segmented-in-series SOFCs by screen printing on flattened tube supports prepared by gelcasting. The processing steps included high-temperature co-firing of the support, anode, electrolyte, and interconnect, followed by application and firing of the cathode. The arrays covered a ≈3.6 cm × 4 cm area, had 12–15 cells on each side of the flattened tubes, a cell length of 1.3 mm, and an interconnect length of 0.2 mm. Print accuracy of the cell active layers to within 0.2 mm was demonstrated using manual visual alignment. Maximum module power output was 8 W at 800 °C. The maximum power density (calculated using active cell area) obtained from a module was ∼700 mW cm^{-2} at 800 °C. Stable operation over 700 h was demonstrated. Excellent array performance stability was measured over 20 redox cycles, presumably due to the small thickness of the Ni-YSZ anodes.

A key area that needs improvement in these devices is the interconnect. The present Pt-YSZ interconnect layers show some gas leakage that was partly responsible for the lower than theoretical open-circuit voltages. Also, the cost of Pt interconnects would be prohibitive for many SOFC applications. Thus, a ceramic interconnect with low materials cost would be a critical improvement for SIS-SOFCs. The interconnect material should be readily screen printed and should reach high density in a co-firing step while not reacting with the other cell components. We are currently testing a number of promising candidate materials for this application. In addition, based on our experience with fabricating the current design, it will also likely be possible to decrease the gap area between individual cells. This will increase the percentage of active cell area from the current value of ∼53 to >60%, thereby increasing power output.

Acknowledgements

The authors thank Tammy Lai, Yi Jiang, Nikkia McDonald, and Negar Mansourian for useful discussions and help with the experimental work. The authors also thank Scott Swartz, Bill Dawson, Mick Day, Ed Sabolsky, Anil Prem, and Dan Kearl for a fruitful collaboration on the segmented-in-series SOFC design and materials. The authors gratefully acknowledge the financial support of the Advanced Technology Program and a Department of Energy Phase II SBIR grant.

References

[1] T.S. Lai, S.A. Barnett, J. Power Sources 147 (2005) 85.
[2] A.O. Isenberg, Solid State Ionics 3/4 (1981) 431;
N.Q. Minh, J. Am. Ceram. Soc. 76 (3) (1993) 563.
[3] F.J. Gardner, M.J. Day, N.P. Brandon, M.N. Pashley, M. Cassidy, J. Power Sources 86 (2000) 122.
[4] J. Iritani, K. Kougami, N. Komiyama, K. Nagata, K. Ikeda, K. Tomida, SOFC VII, in: H. Yokokawa, S.C. Singhal (Eds.), PV 2001-16, The Electrochemical Society Proceedings Series, Pennington, NJ, 2001, p. 63.
[5] D.J. St. Julien, T.D. Ketcham, M.E. Badding, J.L. Brown, P. Diep, K.A. Wexell, R.R. Wusinka, J.E. Cortright, J. Olenick, 2005 Fuel Cell Seminar Abstracts, 2005, p. 73.
[6] T.S. Lai, J. Liu, S.A. Barnett, Electrochem. Solid State Lett. 7 (2004) A78.
[7] T.S. Lai and S.A. Barnett, unpublished results.
[8] M.A. Janney, S.D. Nunn, C.A. Walls, O.O. Omatete, R.B. Ogle, G.H. Kirby, A.D. McMillan, in: M. Rahaman (Ed.), The Handbook of Ceramic Engineering, Marcel Dekker, 1998.
[9] P. Von Dollen, S. Barnett, J Am. Ceram. Soc. 88 (2005) 3361.
[10] F. Zhao, A.V. Virkar, J. Power Sources 141 (2005) 79.
[11] Y.B. Lin, Z.L. Zhan, J. Liu, S.A. Barnett, Solid State Ionics 176 (2005) 1827.
[12] T. Ishihara, in: W. Vielstich, A. Lamm, H. Gasteiger (Eds.), Handbook of Fuel Cells, vol. 4, Wiley, Hoboken, NJ, 2003, p. 1109.
[13] J. Liu, S.A. Barnett, J Am. Ceram. Soc. 85 (2002) 3096.
[14] N.M. Tikekar, T.J. Armstrong, A.V. Virkar, J. Electrochem. Soc. 153 (2006) A654.
[15] G. Stathis, D. Simwonis, F. Tietz, A. Moropoulou, A. Naoumides, J. Mater. Res. 17 (2002) 951.